An Airgun Array Source Model Accounting for High-Frequency Sound Emissions During Firing—Solutions to the IAMW Source Test Cases

Alexander O. MacGillivray, *Member, IEEE*

***Abstract*—JASCO's Airgun Array Source Model (AASM) is a combined deterministic and stochastic model that separately treats the low-frequency and high-frequency components of signals produced by airgun arrays. The low-frequency module is based on solving the equations of motion for interacting spherical bubbles. The high-frequency module is based on a stochastic model of the airgun spectrum, which has been derived from a principal component regression analysis of the experimental data. This stochastic model determines the frequency spectrum of an airgun waveform during the rapid onset of a pressure that occurs when air is released from the gun chamber. AASM combines the output of these two modules to predict the source waveform of an airgun array over a wide frequency range (0–25 kHz). AASM was among the source models included in benchmark comparisons presented at the International Airgun Modeling Workshop (IAMW), held in Dublin, Ireland, in 2016. Results from the workshop showed that different source models agreed reasonably well at low frequencies (<200 Hz), but they diverged substantially at high frequencies (>1 kHz). To help better understand the reasons for a mismatch between source models, this paper presents solutions to the IAMW source test cases, calculated using AASM, as well as a detailed description of AASM's theoretical underpinnings.**

***Index Terms*—Benchmark case, geophysical sources, numerical models, underwater acoustics.**

I. Introduction

THE International Airgun Modeling Workshop (IAMW), held in Dublin, Ireland, in July 2016, provided a set of test problems for validating acoustical models of airgun arrays, with a focus on the environmental effects of sound on marine life. The IAMW test problems included two distinct parts: first, modeling the source output of an airgun array; and second, modeling the propagation of this sound into the environment. This paper focuses only on modeling the source output, and it presents solutions to the three workshop source test cases (S1, S2, and S3) using JASCO's Airgun Array Source Model (AASM, version 1.3beta). Details of the test cases are provided in the workshop problem description [1].

Comparisons of results from different source models, presented at the meeting, showed reasonably good agreement at low frequencies (<200 Hz) but a large mismatch at high frequencies (>1 kHz) [2]. While specific features of the predicted waveforms, such as the rise time, were identified as the cause of the mismatch, the underlying reasons for these differences remains unclear. This paper addresses this latter question by providing solutions to the source test cases and a detailed description of AASM's theoretical underpinnings.

AASM is a numerical model that predicts acoustical source waveforms [3] for the elements of an airgun array, based on the positions, volumes, types, and firing pressures of these elements. It was specifically designed for modeling underwater noise to inform environmental assessments, and thus predicts unfiltered source output over a wide frequency range (0–25 kHz) relevant to marine wildlife [4]. AASM is an integrated model that consists of separate computational modules for predicting the low-frequency and high-frequency output of an airgun array. Its output is tuned against a large library of measured single-gun signatures, with the most recent version of AASM having been tuned against wide-bandwidth hydrophone data from the Svein Vaage broadband airgun study [5]. Source waveforms predicted by AASM are used to calculate the far-field output of an airgun array. In this way, they are conceptually equivalent to notional source signatures derived from near-field measurements, as originally defined by Ziolkowski *et al*. [6].

II. AASM Low-Frequency Module

Because the signature of an airgun is highly repeatable [7] at low frequencies, it is well suited to prediction using physical models. Furthermore, at frequencies where bubble size is smaller than the acoustical wavelength, it is reasonable to approximate the bubble as an isotropic spherical source [6] (while more accurate predictions are possible using three-dimensional computational fluid dynamics codes, as in [8], such methods are considerably more computationally intensive and better suited for modeling single airguns rather than full arrays). AASM calculates low-frequency source outputs using a physical model of spherical bubble oscillation and radiation (based on the approach of Ziolkowski [9]) that also incorporates pressure and motion interactions between guns. Free parameters in the model are tuned against measurements of received sound pressures generated by different airguns obtained under controlled experimental conditions. This section details the physical model implemented by AASM and refers to relevant primary literature sources.

Manuscript received June 29, 2017; revised May 18, 2018; accepted June 28, 2018. Date of publication July 31, 2018; date of current version July 12, 2019.
Guest Editor: M. Ainslie.
The author is with JASCO Applied Sciences, Victoria, BC V8Z 7X8, Canada (e-mail: alex@jasco.com).
Digital Object Identifier 10.1109/JOE.2018.2853199

The individual airgun bubbles are modeled using Gilmore's equation of motion for a large spherical air bubble oscillating in an infinite, compressible, and inviscid liquid [10]. An additional viscous-like damping term $-\alpha u$ is added to Gilmore's equation to simulate energy loss to turbulence

$$\frac{du}{dt} = \left[\left(1+\frac{u}{c}\right)H + \frac{a}{c}\left(1-\frac{u}{c}\right)\frac{dH}{dt} - \frac{3}{2}u^2\left(1-\frac{u}{3c}\right) - \alpha u\right] \Big/ \left[a\left(1-\frac{u}{c}\right)\right] \quad (1)$$

where a is the bubble radius, $u = da/dt$ is the bubble wall velocity, c is the speed of sound in water, H is the enthalpy at the bubble wall, and α is a free constant controlling the turbulent damping. As shown by Prosperetti and Lezzi [11], the Gilmore equation belongs to a family of equations that describe the radial motion of a spherical bubble to first-order accuracy, in terms of the Mach number at the bubble wall. Some form of artificial damping must be introduced in (1) to account for energy lost to turbulence in the isotropic bubble model, since radiative energy loss alone does not account for the observed decay of the airgun bubble oscillations. The thermodynamic properties of the bubble are encapsulated in the enthalpy term, H. Though (1) was derived for compressible water, satisfactory results are obtained by calculating the enthalpy assuming the water density is independent of pressure

$$H = \left(P_{\text{eff}} - P_a\right)/\rho_w \quad (2)$$

where P_a is the pressure at the bubble wall, ρ_w is the water density, and P_{eff} is the effective hydrostatic pressure at the bubble. Following Giles and Johnston [12], the effective hydrostatic pressure at each bubble is the sum of the hydrostatic pressure at depth plus the time-varying pressure fields of adjacent guns in the array.

The airgun bubble is assumed large enough that we may neglect surface tension at the bubble wall, which is small relative to the internal pressure. Following Landrø *et al*. [13], the pressure and temperature of the bubble interior are modeled as an open, quasi-static thermodynamic system in which the energy gained by the bubble, due to mass transfer and heat loss, must be balanced by its change in internal energy. Under these constraints, the time derivative of the internal temperature can be expressed as

$$\frac{dT}{dt} = \left(R_g T\frac{dm}{dt} - \frac{dQ}{dt} - P_a\frac{dV}{dt}\right) \Big/ \left(mc_V\right) \quad (3)$$

where T is the temperature of the bubble interior, R_g is the gas constant, c_V is the heat capacity of air at constant volume, m is the mass of air in the bubble, $V = 4/3\pi a^3$ is the bubble volume, and dQ/dt is the rate of heat transfer into the bubble.

Thermodynamic damping of the bubble oscillation is controlled by the heat transfer term, in a manner similar to Laws *et al*. [14], where it is assumed that the water surrounding the bubble behaves as a temperature reservoir. The rate of heat loss across the bubble wall is assumed to be proportional to the surface area of the bubble and the temperature difference across the interface, which is defined as follows:

$$\frac{dQ}{dt} = \kappa\left[4\pi a^2\ \left(T - T_{\text{wat}}\right)\right] \quad (4)$$

where T_{wat} is the temperature of the water and κ is a constant of proportionality.

The throttling of airflow by the gun ports controls the amplitude and rise time of the initial peak of the pressure signature. Following Laws *et al*. [14], the rate of mass transfer is taken to be proportional to the area of the gun ports, the pressure differential across the gun ports, and the density of air in the chamber. Empirically, good agreement with data is obtained when the following two additional assumptions are employed: The rate of flow through the ports is assumed to vary with chamber volume according to a power law (exponent β), and the total air mass transferred from the chamber to the bubble is controlled by an efficiency parameter $0 < \eta \leq 1$

$$\frac{dm}{dt} = \tau\left(V_{\text{chm}}/V_{\text{ref}}\right)^{\beta}\sqrt{\eta\left(P_{\text{chm}} - P_a\right)\left(m_{\text{chm}}/V_{\text{chm}}\right)} \quad (5)$$

where τ is a port-throttling constant, V_{chm} is the chamber volume, V_{ref} is a reference volume ($1\ \text{m}^3$), P_{chm} is the chamber pressure, and m_{chm} is the air mass inside the chamber.

The pressure and particle motion fields of the oscillating bubbles are computed according to Ziolkowski's quasi-acoustical approximation [9]. Under this approximation, the following two quantities are radiated away from the bubble wall with velocity c

$$f\left(t - a/c\right) = a^2\left(cu - \frac{u^2}{2} - H\right)\Big/ c \quad (6a)$$

$$f'\left(t - a/c\right) = a\left(u^2/2 + H\right) \quad (6b)$$

where $t - a/c$ is the retarded time at the bubble wall. The acoustical pressure and velocity fields at distance r are given in terms of (6) as follows:

$$p\left(t - r/c\right) = \rho_w f'\left(t - r/c\right)/\text{r} - \left(\rho_w u^2\right)/2 \quad (7a)$$

$$v\left(t - r/c\right) = f\left(t - r/c\right)/r^2 + f'\left(t - r/c\right)/rc \quad (7b)$$

where p is the acoustical pressure due to the passing wave and v is the fluid motion in the radial direction between the bubble and the receiver at distance r. Equation (7a) is used to calculate pressure interactions between bubbles [P_{eff} in (2)], and (7b) is used to calculate motion interactions between bubbles. In the latter calculation, the bubble centroids are assumed to move subject to the summed velocity fields of the adjacent bubbles. The equations of motion, and their auxiliary equations, form a system of ordinary differential equations (ODEs) that are solved numerically. Details of the numerical methods that are used for solving the ODE system are provided in [15].

The bubble model contains five free parameters ($\alpha, \beta, \tau, \kappa$, and η) that are constrained by fitting the model predictions to experimental data, using a simulated annealing global optimization algorithm [16] with final quenching using the downhill simplex method [17]. Simulated annealing is effective at finding the global minimum of functions with many local minima because, unlike downhill optimization methods, it avoids getting trapped

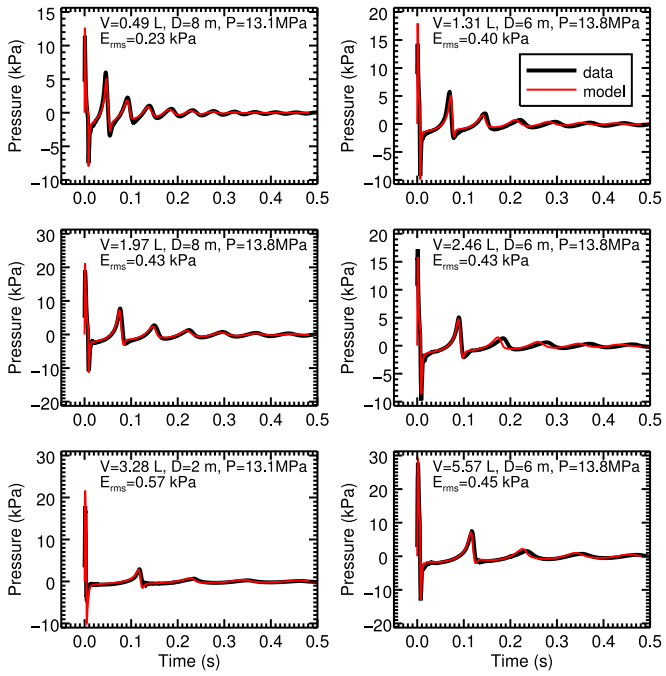

Fig. 1. Plots comparing optimized bubble model predictions with hydrophone measurements of Bolt LL and LLX airguns from the Svein Vaage broadband airgun study. The plot annotations indicate the volumes (V), depths (D), and firing pressures (P) of the airguns, as well as the root-mean-square error between modeled and measured signals (E_{rms}). Received sound pressures from the model are calculated from the predicted source waveforms using the method of images, based on the source–receiver geometry. Peak pressures from the data and model traces have been time-aligned to facilitate comparison.

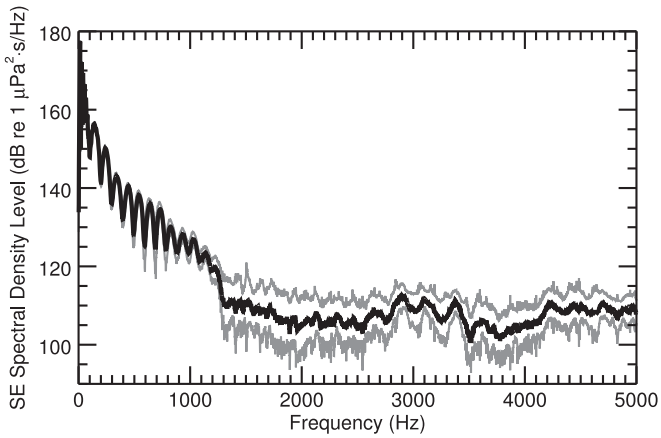

Fig. 2. Mean and standard deviation sound exposure spectral density level of 30 shots from a 3.28 L (200 in^3) Bolt 1900LLX airgun, from the Svein Vaage broadband airgun study, measured at 14.9-m range.

in local minima by randomly accepting trial models in the uphill (greater cost) direction. However, simulated annealing is slow to converge to a true minimum so the simplex method is used as a final step to refine the best-fit solution. The version of AASM that was applied to the workshop problems was tuned to experimental measurements of Bolt LL and LLX airguns, with volumes ranging from 0.49 L (30 in^3) to 5.57 L (340 in^3). For the tuning data set, which consists of 138 different airgun measurements collected at ranges less than 30 m, the root-mean-square error between the optimized bubble model and the measurements is 0.56 kPa. Validation comparisons show that source waveforms calculated by the optimized bubble model are in good agreement with hydrophone measurements of real airguns (see Fig. 1).

III. AASM High-Frequency Module

High-frequency sound emissions are often an undesired byproduct of airgun arrays because they are not useful for seismic imaging, but may nonetheless be audible to marine fauna [18]. Measurements by Landrø *et al*. [19] demonstrated that the acoustical emissions of airgun arrays above 1 kHz can be attributed primarily to two mechanisms. First, the rapid pressure onset during firing; and second, ghost cavitation caused by negative reflections from the sea surface interacting to create clouds of cavitation bubbles several meters below the surface. Mechanism 1 is present for all airgun arrays, regardless of their firing depth or layout, whereas mechanism 2 requires that the array be configured in such a way that the negative sound pressure approaches the cavitation limit in water. Furthermore, in mechanism 2, the ghost cavitation is not at the same location as the airgun bubbles and, thus, it needs to be treated as a separate, spatially-distributed sound source. The high-frequency module in AASM addresses mechanism 1 by shaping the high-frequency spectra of individual airguns in an array using a multivariate statistical model derived from measurements (described below). At the time of writing, AASM does not simulate mechanism 2.

Single-gun measurements show that the repeatability of the airgun spectrum is poor at high frequencies, with large shot-to-shot variability (see Fig. 2). Furthermore, the sound energy at high frequencies is concentrated in a very short time window (<50 ms), centered around the initial pressure peak. While the physical mechanism responsible for the variability in the high-frequency spectrum is not entirely understood, the observed randomness nonetheless suggests that it may be modeled empirically as a stochastic process.

To this end, an empirical model of the high-frequency airgun spectrum was developed and incorporated into AASM, which is described as follows.

1) The high-frequency components of the source signal (0.5–25 kHz) were extracted from a large collection of single-gun data (253 sequences of ∼30 shots each) using a 36-dB/octave highpass filter.
2) A 50 ms period around the peak was windowed out of the filtered signals, and the pressure was multiplied by the receiver range r to obtain the high-frequency source waveform.
3) The mean and ±standard deviation spectra were computed for each shot sequence.
4) A real cepstrum transform [20] was applied to the mean and standard deviation power spectra, retaining only the first 256 cepstrum coefficients (<5.12-ms quefrency). The upper quefrency limit was taken to be smaller than the time delay between the initial pulse onset and the surface reflection, which eliminated modulation of the measured spectrum due to the surface ghost.

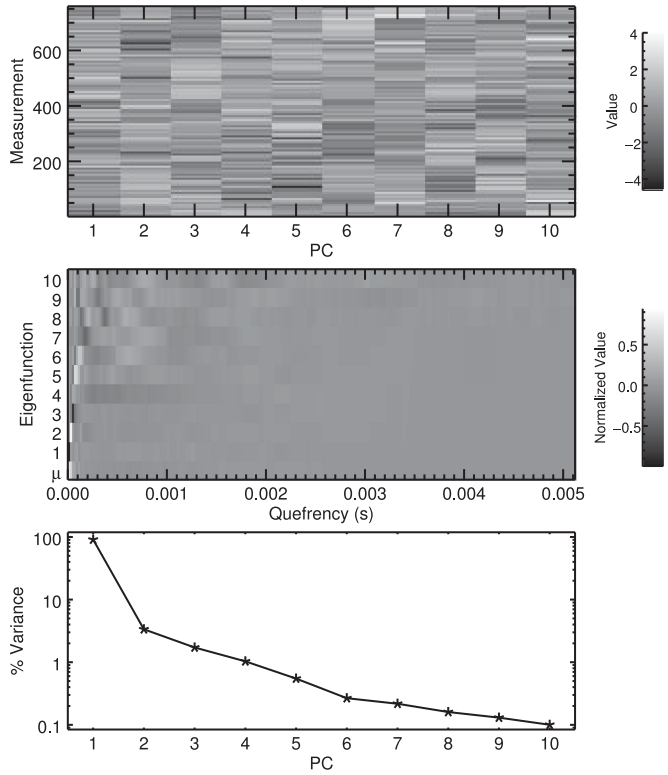

Fig. 3. Top: PC decomposition (PC1 to PC10) of the first 256 cepstrum coefficients for the high-frequency airgun data set. Middle: Cepstrum Eigen functions, and mean, μ, for PC1 to PC10 (normalized for display purposes). Bottom: Percent of data variance explained by PC1 to PC10.

5) Principal component (PC) analysis was applied to the cepstrum coefficients for 759 spectra (mean and $\pm$std. dev. for 253 sequences; see Fig. 3). In total, ten PCs (i.e., derived variables, denoted PC1 through PC10) were retained, accounting for 98.1% of the total data variance.
6) A predictive model was developed using PC regression (PCR) to determine linear relationships between the derived variables and airgun firing parameters.

The dependent variables of the PCR model are: volume V_g, firing depth D_g, and firing pressure P_g. A categorical variable G represents airgun type. A dummy regression variable σ is introduced to account for the random amplitude variation of the spectrum, where the value of the variable corresponds to the mean ($\sigma = 0$) and standard deviation ($\sigma = \pm 1$) spectra. A multiple regression model of the following form is thus fit to each PC

$$\hat{Y}^{(n)} = m_V^{(n)} \log_{10} V_g + m_P^{(n)} \log_{10} \mathrm{P}_g + m_D^{(n)} \log_{10} D_g + m_\sigma^{(n)} \sigma + b_G^{(n)} \quad (8)$$

where n is the PC number, m_X is the slope coefficient of parameter X, and b_G is an intercept coefficient corresponding to the airgun type. Mathematically, the three log-transformed parameters in the regression model (V_g, P_g, and D_g) are converted to nondimensional quantities by dividing by a unit reference value (1 in^3, 1 lbf/in^2, and 1 m, respectively). The predictive power of the regression model was highest for PC1 ($r^2 = 0.82$) and lower for PC2 through PC10 ($r^2 < 0.36$). The residual variability is the component of the spectrum that is not explained by the PCR model. This is interpreted as additional randomness that cannot be predicted from the dependent variables, and it is modeled by introducing a random deviation into the PCR model

$$Y^{(n)} = \hat{Y}^{(n)} + \Delta \times s_Y^{(n)} \quad (9)$$

where Δ is a random variable with standard normal distribution and $s_Y^{(n)}$ is the standard error of the best-fit model for PCn.

The best-fit PCR model [i.e., (8)] predicts high-frequency spectra for single airguns. Shot-to-shot variability is simulated using a Monte Carlo algorithm, where the spectral distribution is sampled by repeated evaluation of (8) and (9), assigning random values to σ and Δ on each iteration ($\sim$300 iterations per PC per airgun are sufficient for most arrays). Note that (8) only predicts the magnitude of the high-frequency spectrum, since the cepstrum discards phase information. Furthermore, while this model treats the high-frequency radiation of the bubble as isotropic, the actual radiation at these frequencies is likely to have directivity, due to deviations from sphericity. The isotropic approximation is nonetheless reasonable in this case because such directivity is likely to vary from shot to shot and, thus, will be smoothed out during the stochastic Monte Carlo simulation.

The high-frequency spectrum from (8) must still be combined with the low-frequency pressure signatures from the physical model to predict the broadband output of an array in the time-domain (i.e., from 0 to 25 kHz). The integrated model uses the mean spectrum from the high-frequency module to adjust the magnitude of the spectrum of the source waveforms predicted by the low-frequency module. In this step, the source waveforms are windowed around the initial peak, and the magnitude of the discrete Fourier transform over a 50-ms period is adjusted to match the stochastic PCR spectrum, with a linear transition from 700 to 900 Hz between the low-frequency and high-frequency predictions (the spectra of measured airguns transition from repeatable to stochastic around 1 kHz). Note that the resulting source waveforms correspond to the mean high-frequency spectrum (i.e., the centroid of the distribution) for each airgun in the array. Thus, a stochastic model is used to shape the spectrum of the initial peak of the source waveforms so that they match experimental measurements.

IV. Workshop Problem Results

Using AASM, source waveforms were calculated for the three workshop sources (see Fig. 4). Briefly, the three source configurations are as follows.

S1) A single 2.53 L (155 in^3) airgun.
S2) A 6-element, single-string array with 21.6 L (1315 in^3) total volume.
S3) A 17-element, three-string array with 54.6-L (3333-in^3) total volume, and 0.5-m (rms) random scatter in the airgun locations.

The nominal array depth is 5 m and the nominal firing pressure is 13 790 kPa (2000 lbf/in^2) in all cases. For comparison, the time alignment of the source waveforms has been shifted such that $t = 10$ ms is the time when the signal first passes above

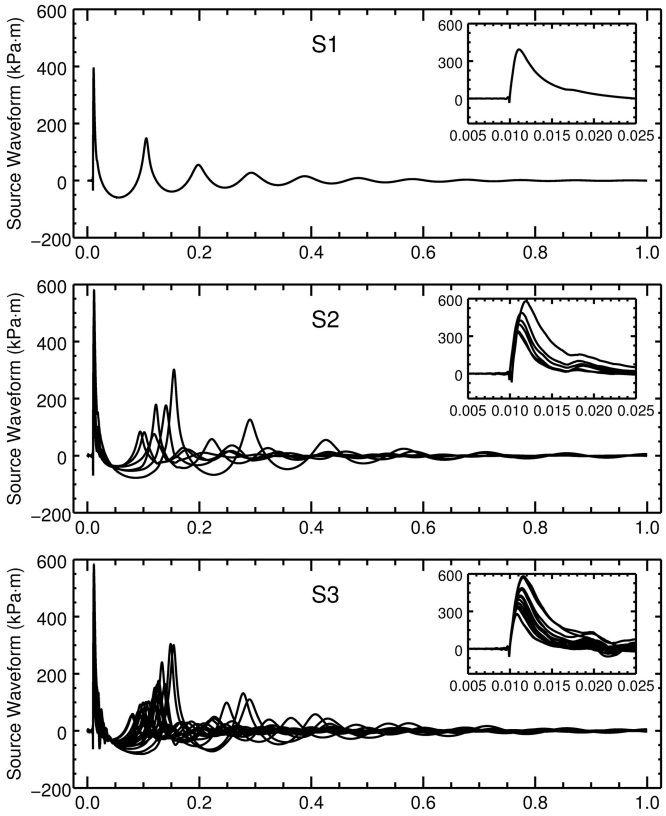

Fig. 4. Source waveforms for the three workshop sources (S1, S2, and S3), as calculated by AASM. Insets show the first 25 ms of the waveforms.

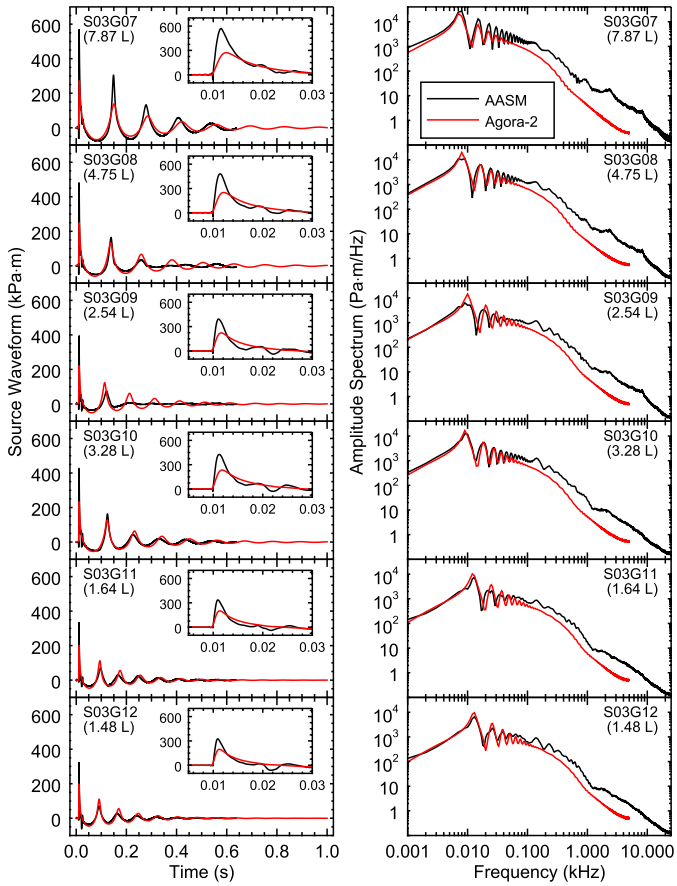

Fig. 5. Comparison of source waveforms (left) and amplitude spectra (right) calculated by AASM and Agora-2, for case the center array of case S3 (sources numbered S03G07–S03G12). Source waveforms from both models have been time-aligned so that the signal crosses 20 kPa·m at $t = 10$ ms. Insets on the left panels show the first 30 ms of the source waveform. Annotations indicate the airgun number from the problem description and the volume of each array element. The AASM source waveforms include airgun–airgun interaction effects, whereas the Agora-2 source waveforms do not.

20 kPa·m. The AASM source waveforms included airgun–airgun pressure interactions for all three source configurations (the choice of whether to model interactions was left to the workshop participants). The reader is referred to the full problem description for additional details [1].

The AASM source waveforms were compared to the Agora-2 source waveforms that were distributed to the IAMW workshop participants (see Fig. 5). Comparisons of the waveforms show that the bubble oscillation periods are in good agreement between the two models, but that the initial peak pressures predicted by AASM are approximately double those of Agora-2. Similarly, comparisons of the spectra show that low-frequency peaks (corresponding to the bubble oscillation periods) are in good agreement between the two models, but that the spectra diverge above 100 Hz, with AASM predicting more high-frequency energy output than Agora-2. Another difference between these two models is that the Agora-2 source waveforms did not include airgun–airgun interactions but AASM did. The interactions manifest themselves as oscillations superimposed on the peak decay during the first tens of milliseconds of the AASM waveforms. However, interactions are of secondary importance in this case and not responsible for the differences in the initial peak pressures. Thus, the main difference between the two models is in the initial pressure onset, which corresponds to the release of air from the gun ports. Differences in the steepness of the initial peaks are also responsible for observed differences in the amplitude spectra above 100 Hz. Differences between AASM and Agora-2 are likely unrelated to AASM's use of the high-frequency module because the two models diverge well below the 700–900-Hz transition band. Two other source models presented at the 2016 IAMW workshop also predicted greater overall high-frequency acoustical output than Agora-2 (see [2] for additional comparisons).

The source waveforms are an intermediate step when calculating the radiated sound field from an airgun array. Most often, the source waveforms of the individual airguns are summed together with appropriate time delays to calculate the far-field source waveform of the array in a specified direction. For the purposes of the IAMW workshop, comparisons between models were performed in terms of the surface-affected source waveform [2], which includes the contributions of surface reflections (i.e., ghosts), assuming a perfectly-flat, perfectly-reflective sea surface. Strictly speaking, the surface reflection is a property of the propagation medium, not of the source; however, including surface reflections in the far-field signature is a common convention in geophysical surveying and is thus useful for comparison purposes. Surface-affected source waveforms (see Fig. 6) and surface-affected amplitude spectra (see Fig. 7)

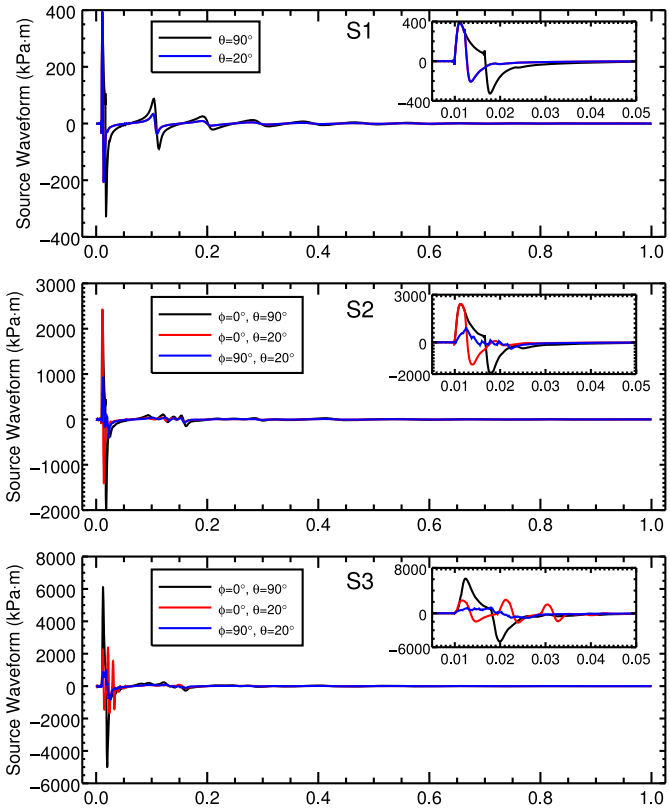

Fig. 6. Surface-affected source waveforms for S1 (top), S2 (middle), and S3 (bottom), as predicted by AASM. Receiver directions are defined such that θ is the angle below the horizontal plane and φ is the angle counterclockwise from the +x axis. Insets show the first 50 ms of the source waveforms.

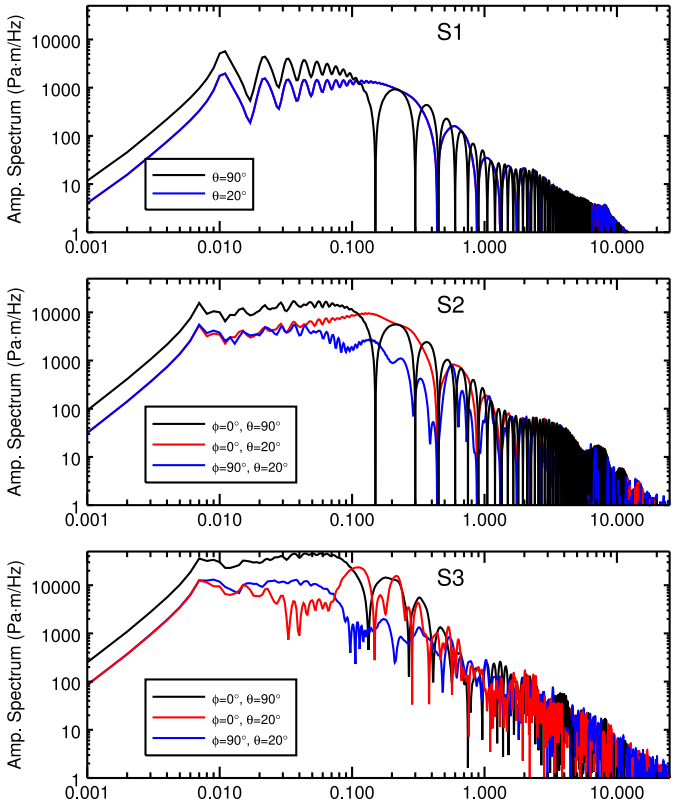

Fig. 7. Surface affected amplitude spectra for S1 (top), S2 (middle), and S3 (bottom), as predicted by AASM. Receiver directions are defined such that θ is the angle below the horizontal plane and φ is the angle counterclockwise from the +x axis.

were calculated from the source waveforms output by AASM for all three workshop sources. However, surface-affected source waveforms should not generally be used with acoustical propagation models since such models generally take a separate account of sea-surface reflections when computing propagation loss.

V. Discussion

Amplitude spectra from the five source models presented at the IAMW were similar at low frequencies (less than 3-dB mismatch below 200 Hz), but deviated substantially at high frequencies (over 30-dB mismatch above 1 kHz) [2]. The differences in the high-frequency model predictions were attributed to differences in the rise times during the first 25 ms of the source waveforms. Predictions from AASM were generally in the middle range of the source models presented at IAMW. Two possible reasons for the observed mismatch between the different source models are: First, differences in tuning data sets; and second, differences in the port-throttling physics. The high-frequency mismatch between models highlights the need for validating model predictions against measurements.

The high-frequency sound emissions (>1 kHz) of airgun arrays are difficult to predict accurately for several reasons. First, the sources themselves are designed to be used at low frequencies, and any high-frequency emissions are generally an unintended side effect (although a new type of airgun attempts to address this issue [21]). Second, the simplified model of an expanding spherical bubble may not adequately capture bubble behavior in the first few milliseconds after an airgun is fired (e.g., due to the asymmetry of the gun ports and vibrations induced by solenoid actuation [22]). Third, sounds generated by nonlinear effects, such as ghost cavitation, are not yet fully understood, though some recent progress has been made by Khodabandeloo *et al*. [23].

The stochastic PCR model implemented in AASM attempts to address the first two issues by a way of an empirical approach that does not depend on an in-depth understanding of the underlying physical phenomena. Nonetheless, developing an empirical model depends on the availability of a substantial collection of high-quality signature data (e.g., [5]). AASM does not yet account for nonlinear cavitation effects that lead to additional high-frequency emissions for multigun arrays. Accounting for these nonlinear effects would permit more accurate predictions of sound emissions for large airgun arrays at frequencies above 1 kHz.

Acknowledgment

The author would like to thank the International Oil and Gas Producers Joint Industry Program on E&P Sound and Marine Life, and specifically J. Campbell (OGP) and M. Jenkerson (ExxonMobil), for making available acoustical data from the Svein Vaage single gun signature measurement project that was

used to calibrate the airgun models described in this work. The author would also like to thank Dr. M. Ainslie (JASCO) and two anonymous reviewers for providing a number of helpful comments that substantially improved the final version of this manuscript.

REFERENCES

[1] M. A. Ainslie, R. M. Laws, and H. Ö. Sertlek, "International Airgun Modelling Workshop: Validation of source signature and sound propagation models—Dublin (Ireland), 16 July 2016—Problem description," *IEEE J. Ocean. Eng.*, vol. 44, no. 3, pp. 565–574, Jul. 2019.

[2] M. A. Ainslie *et al.*, "Verification of airgun sound field models for environmental impact assessment," *Proc. Meetings Acoust.*, vol. 27, 2016, Art. no. 070018.

[3] *Underwater Acoustics—Terminology, Int. Org. Standardization*, ISO/DIS 18405.2:2017, Geneva, Switzerland, 2017, p. 62.

[4] B. L. Southall *et al.*, "Marine mammal noise exposure criteria: Initial scientific recommendations," *Aquatic Mammals*, vol. 33, pp. 411–521, 2007.

[5] A. Mattsson, G. Parkes, and D. Hedgeland, "Svein Vaage broadband air gun study," in *The Effects of Noise on Aquatic Life*, A. N. Popper and A. Hawkins, Eds., New York, NY, USA: Springer-Verlag, 2012, pp. 469–471.

[6] A. Ziolkowski, G. Parkes, L. Hatton, and T. Haugland, "The signature of an air gun array: Computation from near-field measurements including interactions," *Geophysics*, vol. 47, pp. 1413–1421, 1982.

[7] B. F. Giles, "Pneumatic acoustic energy source," *Geophys. Prospecting*, vol. 16, pp. 21–53, 1968.

[8] D. Gerez, H. Groenaas, O. P. Larsen, M. Wolfstirn, and M. Padula, "Controlling air-gun output to optimize seismic content while reducing unnecessary high-frequency emissions," in *Proc. SEG Tech. Program Expanded Abstracts*, 2015, pp. 154–158.

[9] A. Ziolkowski, "A method for calculating the output pressure waveform from an air gun," *Geophys. J. Royal Astron. Soc.*, vol. 21, pp. 137–161, 1970.

[10] F. R. Gilmore, *California Institute of Technology, and Hydrodynamics Laboratory, the Growth or Collapse of a Spherical Bubble in a Viscous Compressible Liquid*. Pasadena, CA, USA: California Inst. Technol., 1952.

[11] A. Prosperetti and A. Lezzi, "Bubble dynamics in a compressible liquid. Part 1. First-order theory," *J. Fluid Mech.*, vol. 168, pp. 457–478, 1986.

[12] B. F. Giles and R. C. Johnston, "System approach to air-gun array design," *Geophys. Prospecting*, vol. 21, pp. 77–101, 1973.

[13] M. Landro, "Modeling of GI gun signatures," *Geophys. Prospecting*, vol. 40, pp. 721–747, 1992.

[14] R. M. Laws, L. Hatton, and M. Haartsen, "Computer modeling of clustered airguns," *First Break*, vol. 8, pp. 331–338, 1990.

[15] A. O. MacGillivray, "Acoustic modelling study of seismic airgun noise in queen charlotte basin," M.Sc. thesis, School of Earth and Ocean Sci., Univ. Victoria, Victoria, BC, Canada, 2006.

[16] S. Kirkpatrick, C. D. Gelatt, and M. P. Vecchi, "Optimization by simulated annealing," *Science*, vol. 220, pp. 671–680, 1983.

[17] J. A. Nelder and R. Mead, "A simplex method for function minimization," *Comput. J.*, vol. 7, pp. 308–313, Jan. 1, 1965.

[18] J. C. Goold and P. J. Fish, "Broadband spectra of seismic survey air-gun emissions, with reference to dolphin auditory thresholds," *J. Acoust. Soc. Amer.*, vol. 103, pp. 2177–2184, 1998.

[19] M. Landrø, L. Amundsen, and D. Barker, "High-frequency signals from air-gun arrays," *Geophysics*, vol. 76, pp. Q19–Q27, 2011.

[20] A. V. Oppenheim and R. W. Schafer, *Discrete-Time Signal Processing*, 2nd ed. Englewood Cliffs, NJ, USA: Prentice-Hall, 1999.

[21] E. Coste *et al.*, "Attenuated high-frequency emission from a new design of airgun," in *Proc. SEG Tech. Program Expanded Abstracts*, 2014, pp. 132–137.

[22] J. Langhammer and M. Landrø, "High-speed photography of the bubble generated by an airgun," *Geophys. Prospecting*, vol. 44, pp. 153–172, 1996.

[23] B. Khodabandeloo, M. Landrø, and A. Hanssen, "Acoustic generation of underwater cavities—Comparing modeled and measured acoustic signals generated by seismic air gun arrays," *J. Acoust. Soc. Amer.*, vol. 141, pp. 2661–2672, 2017.

Alexander O. MacGillivray (M'18) was born in Victoria, BC, Canada, in 1977. He received the B.Sc. (honors) degree in physics and the M.Sc. degree in earth and ocean sciences from the University of Victoria, BC, Canada, in 2000 and 2006, respectively.

He is currently a Senior Scientist and Project Manager with JASCO Applied Sciences, Victoria, BC, Canada, where he has been employed since 2001. He is the primary author of JASCO's Airgun Array Source Model. His research interests include computational methods for predicting underwater noise, underwater ambient noise measurement, and the environmental effects of noise on marine life.